Flow-Based Surface Decoration of Microparticles with Titania and Other Transition Metal Oxide Nanoparticles

L. Zane Miller[1], James J. Rutowski[2], Jonathan A. Binns[2], Guillermo Orts-Gil[3], D. Tyler McQuade[1] and Jeremy L. Steinbacher[2*]

[1]Department of Chemistry and Biochemistry, Florida State University, 95 Chieftan Way, Tallahassee, Florida 32306, USA
[2]Department of Chemistry and Biochemistry, Canisius College, 2001 Main Street, Buffalo, New York 14208, USA
[3]Department of Biomolecular Systems, Max Planck Institute of Colloids and Interfaces (MPIKG), Potsdam-Golm Science Park, Am Mühlenberg 1 OT Golm, Potsdam D-14476, Germany

Received: 12 January 2016; accepted: 07 March 2016

We present a rapid approach for forming monodisperse silica microcapsules decorated with metal oxide nanoparticles; the silica–metal oxide composites have a hierarchical architecture and a range of compositions. The details of the method were defined using titania precursors. Silica capsules containing low concentrations of titania (<1 wt. %) were produced via an interfacial reaction using a simple mesofluidic T-junction droplet generator. Increasing the titania content of the capsules was achieved using two related, flow-based postsynthetic approaches. In the first approach, a precursor solution containing titanium alkoxides was flowed through a packed-bed of capsules. The second approach provided the highest concentration of titania (3.5 wt. %) and was achieved by evaporating titanium precursor solutions onto a capsule packed-bed using air flow to accelerate evaporation. Decorated capsules, regardless of the method, were annealed to improve the titania crystallinity and analyzed by optical microscopy, scanning electron microscopy (SEM), transmission electron microscopy (TEM), energy dispersive X-ray spectroscopy (EDX), powder X-ray diffraction (PXRD), and Fourier transform infrared (FT-IR) spectroscopy. The photocatalytic properties were then compared to a commercial nanoparticulate titania, which the microcapsule-supported titania outperformed in terms of rate of degradation of an organic dye and recyclability. Finally, the generality of the flow-based surface decoration procedures was demonstrated by synthesizing several composite transition metal oxide–silica microparticle materials.

Keywords: microcapsules, micro-/mesofluidics, photocatalysis, metal oxide nanoparticles, silica

1. Introduction

Hollow inorganic spheres and capsules are key components in many applications including industrial fillers, adsorbents, drug delivery vehicles, microreactors, optical technologies, and catalysts [1–5]. Pure silica and titania capsules have been well-studied and applied, but less is known about the preparation and application of composite SiO_2–TiO_2 capsules [6–11]. Although composite capsules are less known, a number of reports suggest that these mixed oxide materials have broad use in areas ranging from waste water remediation to dye-sensitized solar cells [12–14]. The most conventional synthetic methods to generate hollow silica–titania materials use either hard or soft templates. Hard templating [8, 9, 15–17] is achieved by assembling layers of material onto a solid template before the solid is removed using heat or solvents once the assembly is complete. The hard templating approach is often used to prepare monodisperse capsules. Conversely, soft templating [18–22] uses a droplet as a template and tends to enable more rapid and scalable synthesis of particles. While batch methods are cost-effective and fast compared to hard-templating, the approach often yields a broad distribution in capsule size.

On the other hand, continuous formation of droplets using flow-based techniques is now widely used to generate monodisperse, micron-sized droplets that can produce monodisperse capsules or particles via a soft-templating approach [23, 24]. We and others have demonstrated the utility of simple devices for the formation of droplets and microcapsules from reactive precursors [25–28]. While using tubing and T-junctions provides an uncomplicated alternative to chip-based devices, the approach also enables rapid device reconfiguration that can offer new capabilities. For example, we have demonstrated that monodisperse SiO_2 capsules were readily formed using a flow-based droplet system via tuned interfacial condensation [26]. The key in our prior system was that we used alcohol additives to tune the interfacial condensation rate. We hypothesized, and present work here validating this idea, that we could use a similar approach to produce composite SiO_2–TiO_2 capsules. As we describe in more detail below, we succeeded, but were unable to identify a set of conditions that enabled direct formation of composite capsules from disperse-phase solutions containing more than 2.5 mol % Ti precursor.

We hypothesized that capsules containing higher loadings of TiO_2 could be achieved by postsynthetic functionalization using a second flow-based device. In particular, we proposed that pure SiO_2 or 2.5 mol % SiO_2–TiO_2 capsules packed into a column could be decorated with TiO_2 by flowing precursor solutions around the capsules without destroying the integrity of the shells (whereas use of a magnetic stir bar in a batch reactor destroys the shells). We predicted that capsules could be decorated using two related approaches: (1) flowing reactive solutions of titania through a capsule packed-bed or (2) evaporating reactive species onto the capsules in a capsule packed-bed.

Herein, we demonstrate that SiO_2–TiO_2 composite materials can be created in flow and postsynthetically decorated with TiO_2 using a second, packed-bed flow system. These simplified systems enabled both the rapid formation of SiO_2–TiO_2 microcapsules (seconds) and subsequent surface decoration of the formed capsules using small-scale, continuous-flow or semi-continuous evaporative approaches (Figure 1). Annealing the composite capsules provided anatase crystallites on the outer surface of the silica shells that were effective catalysts for the photodegradation of an organic dye. We demonstrated the generality of our flow-based surface decoration technique by coating a variety of transition metal oxide nanoparticles onto silica microparticles using the same strategy.

* Author for correspondence: steinbaj@canisius.edu

DOI: 10.1556/1846.2016.00002

First published online: 13 April 2016

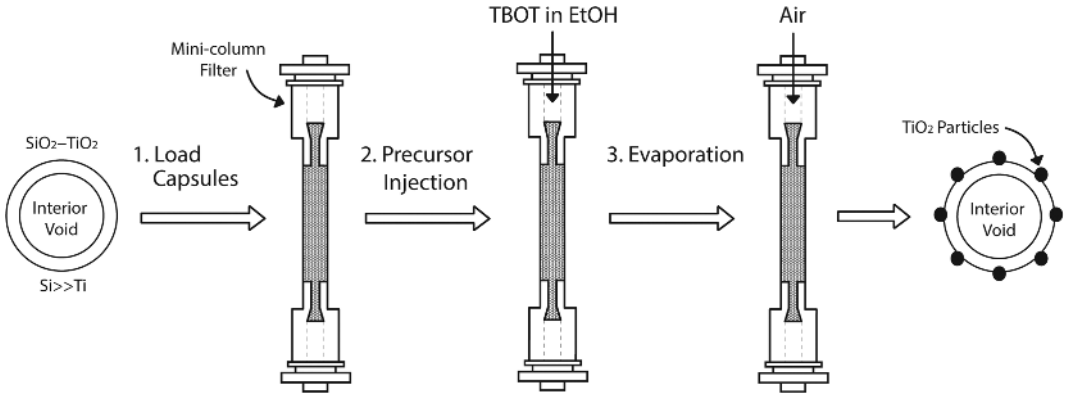

Figure 1. Illustration of the flow-evaporation method of decorating the microcapsules with titania particles. The hollow shells are loaded into the cartridge, solutions of titanium alkoxides (or other transition metal salts) in ethanol are injected into the cartridge, and air flow is used to evaporate the solvent, dispersing TiO_2 onto the surface. The continuous-flow process follows a similar approach, but heat is applied to the cartridge to form TiO_2 coatings over a period of 4–5 h (no air flow used)

2. Results and Discussion

2.1. Synthesis of Mixed Silica–Titania Shells via Interfacial Condensation. Previous work in our laboratory demonstrated that fast-reacting precursors such as $SiCl_4$ could be used to create microcapsules by tuning the condensation rate using alcohol additives [26]. Formation of HCl gas upon fast hydrolysis of the Si–Cl bonds served to create the void around which the interfacial polymerization proceeded, leaving behind the inorganic shell. Water remained in contact with the interface, initiating further hydrolysis and subsequent condensation, leading to thicker shells as the capsules approached and exited the tubing. We sought to apply this approach to prepare silica–titania composite materials. Using our previously described simple droplet maker [26], we began to study the condensation of mixed silica and titania precursors.

To our satisfaction, mixtures of TEOS, $SiCl_4$, and titanium alkoxides yielded well-formed capsules when the concentration of titanium precursors was kept below 2.5 mol % (Figure 2). Above this concentration, self-supporting capsules did not form; instead, unstructured precipitates formed. Visual inspection of the system showed that at higher concentrations of titania precursor, the rate of the hydrolysis and condensation reactions was much faster than the droplet formation step. This is perhaps unsurprising because the rate of hydrolysis for Ti alkoxides is more than five orders of magnitude faster than for Si alkoxides [29]. Indeed, solution-phase ^{29}Si nuclear magnetic resonance (NMR) spectroscopy confirmed that rapid exchange of chloride and ethoxy groups occurred between TEOS and $SiCl_4$ within 10 min after the preparation of the disperse-phase solution (Figure S1). This is even faster than in our previous report of purely silica microparticles that did not use titanium alkoxides [26].

Attempts to slow down the rapid condensation reaction through changes to the continuous phase (viscosity, water content, etc.) or dilution of the disperse phase with ethanol, *n*-butanol, or *n*-hexanol did not lead to the same rapid formation of capsules as in our previous studies. When the disperse phase was diluted with these alcohols, droplet formation became achievable, yet rapid formation of solid shells did not occur. Instead, the droplets reached the collection bath and readily burst without leading to self-supporting capsules.

Optical microscopy was used for initial inspection of the transparent shells formed from up to 2.5 mol % Ti alkoxide solutions after aging 10 min in collection bath (Figure 2). Differences in shell morphology were apparent compared to microcapsules made without Ti precursors [26]. The shells of the capsules appeared to have an additional thin layer of material. We speculated based upon these initial observations that TiO_2 could be present as a single thin layer. The variation in size

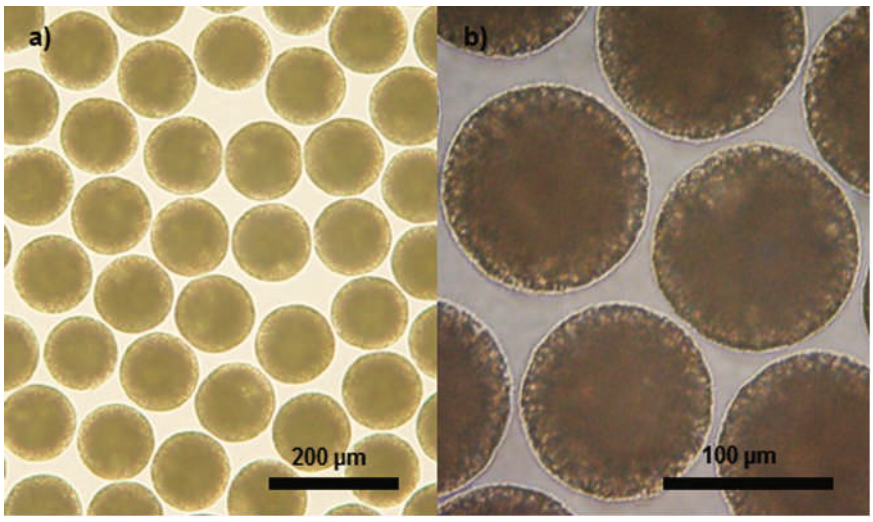

Figure 2. Optical microscope images of capsules produced from disperse-phase droplets with a composition of 0.5 mL $SiCl_4$ + 0.93 mL TEOS + 0.12 mL *t*-butanol + 70 µL TBOT (molar ratio: 1.0:0.93:0.06:0.05; disperse-phase flow rate = 35 µL/min) formed in a continuous phase composed of 80% glycerol + 20% deionized water (flow rate = 2.00 mL/min). The capsules were collected directly onto a clean microscope slide and imaged

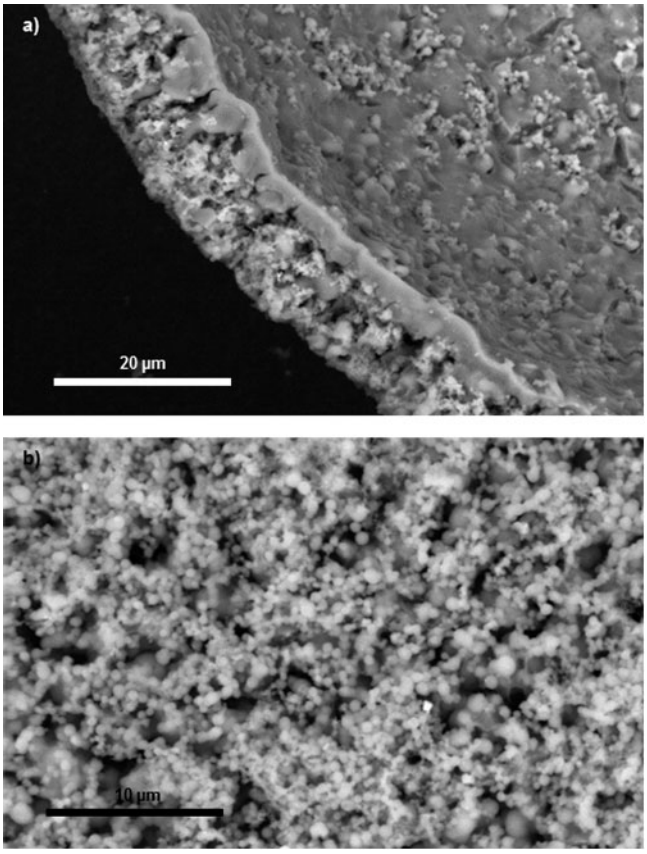

Figure 3. Scanning electron microscope images of a halved capsule (a; scale bar = 20 μm), and the outer surface of the capsule which is covered with aggregated small particles (b; scale bar = 10 μm)

was determined for samples of capsules immediately after exiting the tubing. The coefficient of variation (ImageJ software) was observed to be 3.8 %, which is consistent with the results in our previous work using simple tubing-based devices [26].

Scanning electron microscopy (SEM) revealed the morphology of the shells in greater detail (Figure 3 and Figures S7–9). The outermost portion of the shells of the capsules appeared to be composed of aggregated particles (100 nm to 1 μm in size), and a capsule which had split in half displayed the dense inner shell covered with small particles on the surface (Figure 3a and b). We speculate that this hierarchical structure formed via a mechanism similar to our previous report using organosilane precursors [25]. Rapid hydrolysis and condensation of the most reactive precursor molecules – namely $SiCl_4$ – likely formed the dense inner shell first. Subsequently, the surficial nanoparticles formed when further silica and titania precursor molecules underwent hydrolysis, condensation, and growth via a mechanism similar to the well-known Stöber synthesis of silica particles [30].

Other techniques demonstrated that both silica and titania were incorporated in the composite materials. SEM–energy dispersive X-ray spectroscopy (EDX) elemental mapping (Figure 4) confirmed the presence of titanium, silicon, and oxygen on the surface of the shells before subsequent TiO_2 decoration steps. TEM revealed that TiO_2 nanoparticles were distributed throughout the shells (Figure S6). Also, EDX point mapping of the undecorated capsules was used to demonstrate that the concentration of Ti was low (~1 atom. % by EDX), consistent with the low mole percent of titanium alkoxide in the disperse phase (Figure S5, top). Fourier transform infrared (FT-IR) spectroscopy experiments (Figure S10) revealed vibrations associated with –OH, H_2O, and Si–O bonding, though bonds involving titanium species could not be discerned given the low concentrations of Ti [31, 32]. Lastly, powder X-ray diffraction (PXRD) studies of the capsules with titania incorporated solely via interfacial reaction indicated only amorphous material, even upon annealing at 900 °C for 5 h (Figure S3b).

While hierarchically structured composite capsules produced with the single-step, interfacial reaction in a microfluidic device T-junction were interesting, a procedure enabling the incorporation of higher percentages of metal oxide would increase the potential applications of these materials. With this goal in mind, we began to seek an engineering-based solution to the problem. Aware of spray-coating and evaporative approaches for formation of multilayered and decorated particles or substrates [33–35], we developed a packed-bed, flow-based approach to achieve the same result.

2.2. Decorating Capsule Packed-Beds Using a Continuous Deposition Approach. SiO_2–TiO_2 capsules prepared from 2.5 mol % TBOT precursor solutions were loaded into

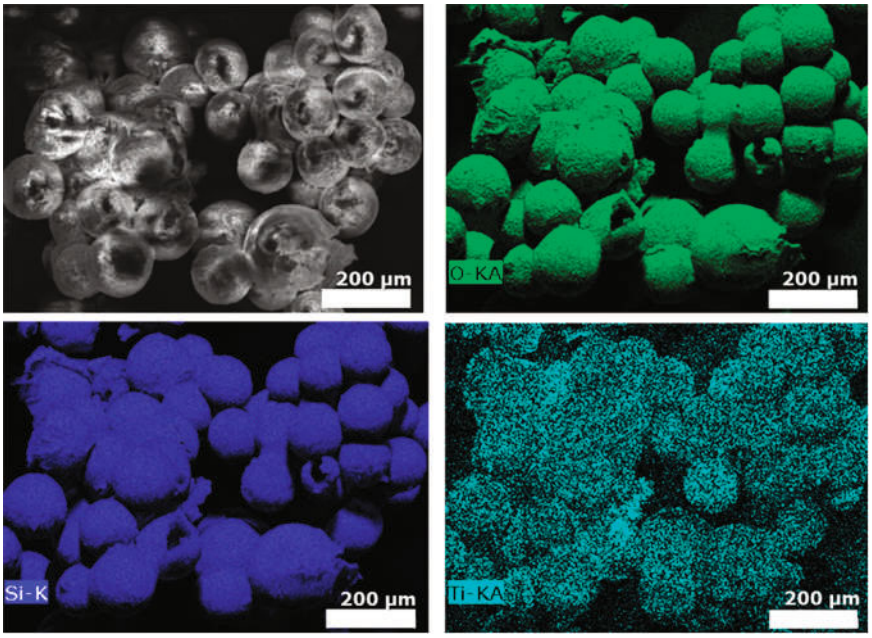

Figure 4. SEM–EDX elemental mappings of capsules produced from disperse-phase droplets of 0.5 mL $SiCl_4$ + 0.93 mL TEOS + 0.12 mL *t*-butanol + 70 μL TBOT (molar ratio: 1.0:0.93:0.06:0.05) prior to performing decoration procedures

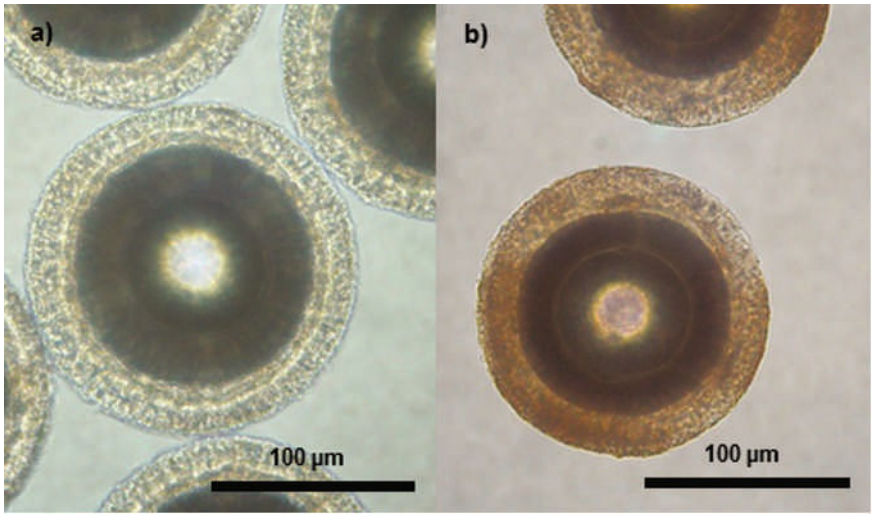

Figure 5. Optical microscope images of unmodified (a) and 0.15 M TBOT 5 h continuous-flow decorated capsules (b) after the sets were annealed at 600 °C for 5 h. Compared to the unmodified microcapsules, the shells of continuously decorated and annealed samples lost optical transparency

cartridges for overcoating experiments (Figure 1, Figure S13). In the first method, the cartridge of capsules was first rinsed with ethanol that had been made slightly basic (pH~8–9). This treatment served to activate the surface for subsequent loading of TiO_2 by hydrolyzing some of the surficial silica, increasing the density of reactive silanols. A solution of 0.15 M TBOT in ethanol was then flowed through the packed-bed of capsules at flow rates of up to 0.200 mL/min using a syringe pump. For comparison, a second procedure was performed without first activating with basic ethanol prior to introduction of the Ti precursor solution. Optical microscopy of the continuously decorated particles showed an obvious densification of the capsule shells compared to the original, nondecorated particles (Figure 5, b versus a).

FT-IR analysis of the continuous-flow decorated capsules from both methods, prior to annealing, revealed similar peaks to the unmodified capsules. After annealing, peaks corresponding to –OH and H_2O vibrations decreased in intensity and the peaks at 580 and 965/cm disappeared, becoming broad shoulders of neighboring signals. After annealing at 600 °C, the capsules were also analyzed by PXRD. Only small features were observed in the patterns corresponding to the 101 and 200 facets of anatase TiO_2 (Figure 6a and Figure S2). Interestingly, the capsules decorated without the basic ethanol prewash displayed the most intense peaks in PXRD experiments of continuous-flow decorated capsules. Reannealing at 800 °C for 5 h led to formation of crystalline SiO_2 and mixed rutile and anatase phases for the microcapsules prewashed with basic ethanol (Figure S3a), but the continuous-flow method without the basic ethanol

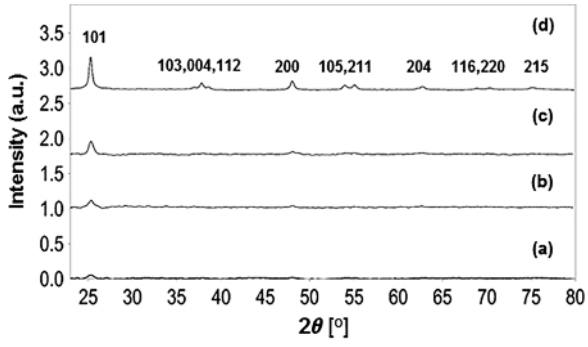

Figure 6. PXRD patterns (background subtracted) of 0.15 M TBOT 5 h continuous-flow decorated (a), 0.10 M TBOT×6 flow-evap. coated (b), 0.15 M TBOT×6 flow-evap. coated (c), and 0.50 M TBOT×6 flow-evap. coated (d) microcapsules annealed at 600 °C

prewash yielded only anatase TiO_2 even after annealing at 800 °C for 5 h. While these methods enabled low TiO_2 loadings (0.25–0.5 wt. %) without destroying the integrity of the shells, the time necessary to complete the process was still on the order of most batch processes (2–5 h). We thus sought a method that would enable a higher titania loading while also requiring less time.

2.3. Decorating Capsule Packed-Beds Using a Flow-Evaporation Approach. We speculated that evaporation of titania precursor solutions directly onto capsules within a packed bed might yield higher loadings of titania particles. To test this hypothesis, we wet the packed-bed with TBOT in ethanol followed by evaporation of the solutions using a flow of air (~2 psi). We rationalized that this method would require less material (solvent and Ti precursor) and time while achieving higher loadings of TiO_2. Indeed, when the concentration of TBOT and the number of coating steps were increased, the particles became less transparent until very little/no light could be observed to pass through the shells (Figure 7). The shells remained relatively smooth, but became rough along the edges as the concentration of Ti precursor was increased. Gratifyingly, EDX point mapping showed a 9-fold increase in Ti content on the microcapsule surfaces (10 atom %) compared to undecorated samples after six consecutive flow/evaporation steps ("×6 flow-evap.") with 0.5 M TBOT (Figure S5, bottom vs uncoated, top).

FT-IR and PXRD were again used to characterize these flow-evaporated materials. As expected, annealing caused the peaks corresponding to –OH and H_2O vibrations to decrease in intensity, and Ti bonding features were likely hidden among the large Si–O vibrations due to low concentrations of TiO_2 (Figure S10). PXRD studies after decorating the materials using the rapid flow-evaporation method and annealing at 600 °C revealed features corresponding to anatase TiO_2. Additionally, the amount of TiO_2 loaded onto the microcapsules using the flow-evaporation method was influenced by both the concentration of precursor and number of steps in the decoration process. As the concentration of TBOT was increased from 0.075 to 0.5 M with the number of coating steps held constant, peaks corresponding to anatase TiO_2 became significantly more intense after annealing (Figure 6). The intensity and number of peaks corresponding to anatase TiO_2 were also improved as the number of coating steps was increased from 3 to 12 (Figure 8). Therefore, this method provided control of TiO_2 loadings (from ~0.2 to 3.5 wt. %) by modulating the concentration of Ti precursor or the number of decoration steps (Table S1). Importantly,

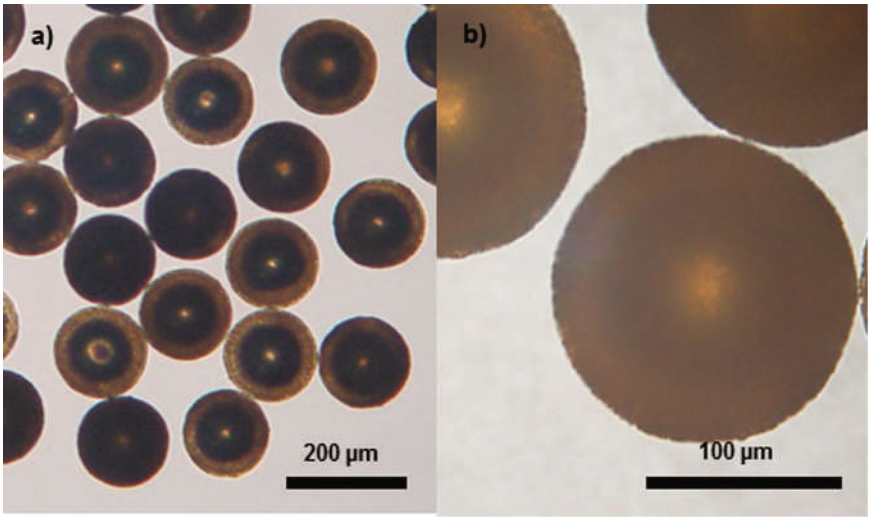

Figure 7. Optical microscope images of 0.5 M TBOT×6 flow-evap. decorated capsules after being annealed at 600 °C for 5 h. Compare to the uncoated SiO_2–TiO_2 particles in Figure 5 (a)

the degree of modification appeared to be consistent from top to bottom of the cartridge, as demonstrated by PXRD data obtained from material recovered from either the upper or lower half of a cartridge (Figures S2 and S4). We calculated the average size of the TiO_2 crystallites by applying the Scherrer equation to the PXRD data. The 0.15 M×12 and 0.5 M×6 TBOT decorated capsules displayed average crystallite sizes of 28 and 25 nm, respectively.

2.4. Photocatalytic Degradation of Methyl Orange (MO). To demonstrate that these materials are suitable for catalytic applications, we used them as a catalyst for the photodegradation of MO, a dye commonly used in such studies [36]. Importantly for photocatalysis, the TiO_2 on these particles is predominantly anatase (see above), which performs better as a photocatalyst compared to other phases due to slower charge recombination and greater electron mobility [36–38]. To showcase the dimensions of the composite particles – relatively large compared to the TiO_2 nanocrystals themselves – we ran these experiments in a miniature packed-bed reactor. The particles were immobilized in a quartz flow cell (0.50 mm beam length) in a photochemical reactor, and solutions of MO were flowed over them using a peristaltic pump. For these studies, we selected the 0.5 M TBOT×6 decorated capsules (3.5 wt. % TiO_2), and the 8.5 mg of immobilized microparticles equated to 300 µg of TiO_2 in the cell. The concentration of MO dye was monitored by ultraviolet–visible (UV–vis) spectroscopy as the flowing solution was exposed to UV light. We assumed that the conditions were pseudo-first-order in [MO], and a plot of ln ($[MO]_t/[MO]_o$) vs. time yielded an apparent rate constant, k, of $7.6 \pm 0.3 \times 10^{-5}$/s (Figure 9, black line).

For comparison, we used commercially available P25 TiO_2 nanoparticles (Degussa, ~21 nm in diameter) as a reference material that is commonly employed in photocatalytic studies [38, 39]. Here, we used the same flow cell setup, but the P25 nanoparticles were instead homogenously dispersed in the MO solution. The mass of P25 TiO_2, 300 µg, was the same as with the decorated capsules, and the apparent rate constant under these conditions was $5.4 \pm 0.6 \times 10^{-5}$/s (Figure 9, gray line). Thus, the capsule-supported TiO_2 appears to be more efficient at the photodegradation of MO than the commercial P25 by a factor of 1.4-fold on an equivalent mass basis. Importantly, these results demonstrate that the surface-decorated TiO_2 nanoparticles were accessible to solvent and reactive molecules therein. Lastly, we explored the reusability of the immobilized capsules by using a single sample in seven consecutive runs spanning 7+ hours of photodegradation (Figure S11). The photocatalytic efficiency was apparently not diminished over this time span, allowing for continuous-flow operation in a variety of future applications. In contrast, the nanoparticulate P25, lacking a solid support, remained inseparable from the degraded MO solution, drastically hampering reusability unless the entire solution was subjected to centrifugation.

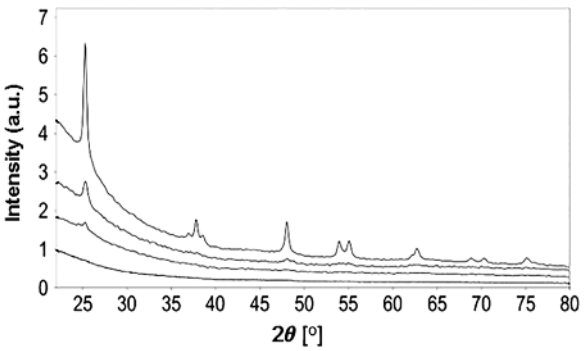

Figure 8. PXRD patterns of 0.15 M TBOT flow-evap. ×12, ×9, and×3 coated microcapsule sets (top to bottom, respectively) annealed at 600 °C for 5 h. Additionally, a pattern for unmodified microcapsules annealed at 900 °C for 5 h is included (bottom pattern)

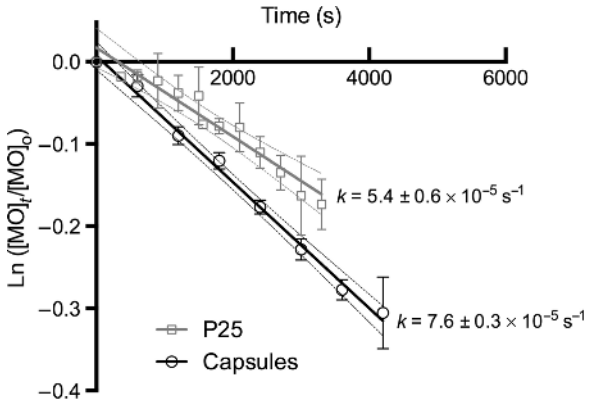

Figure 9. Photodegradation of MO using 0.5 M TBOT flow-evap. ×6 decorated capsules annealed at 600 °C (circles, black) and Degussa P25 nanoparticle (squares, grey) as photocatalysts. We plotted ln($[MO]_t$/$[MO]_o$) vs. time to extract the apparent rate constants, k. Error bars represent the standard deviation of 2–3 data points at a given time, and the dashed lines represent the 95% confidence interval in the linear regression analyses of each data set

2.5. Flow-Evaporation Coating with Other Transition Metal Oxides. Besides titania, many different transition metal oxide nanoparticles have exhibited useful physical and chemical properties, including CuO [40–42], Co_3O_4 [43, 44], Fe_2O_3 [45–47], and NiO [48–50]. Thus, to demonstrate the generality of the flow-evaporation coating procedure, we used the method to surface decorate silica microcapsules with several other transition metal oxide nanoparticles. As before, we loaded silica microparticles – previously prepared by an interfacial reaction in a mesofluidic device – into the cartridge system shown in Figure 1 and Figure S13. Then, soluble metal precursors were introduced from saturated methanolic solutions, and evaporation of the solvent left transition metal salts on the microparticles. A second round of deposition and evaporation was followed by calcination at 660 °C to yield metal oxide nanoparticles coated on the silica microparticles; we prepared samples containing α-Fe_2O_3, CuO, Co_3O_4, and NiO nanoparticles. Unlike titania, the obvious color change induced by the transition metal salts and their oxides provided visual evidence of the deposition and subsequent formation of the oxides (Figures S12 and S13). We characterized the resulting composites by PXRD. All of the diffractograms gave well-resolved peaks for the metal oxide nanoparticles (Figures S14–17), and application of the Scherrer equation provided estimated crystallite sizes of 33 nm (CuO), 38 nm (α-Fe_2O_3), 33 nm (Co_3O_4), and 27 nm (NiO), all in the size range (few× 10 nm) of catalytically active nanoparticles from the literature [38, 40, 44]. Together, these results confirm that our flow-based approach to decorating microparticles with metal oxide nanoparticles is general, given that a soluble salt for that metal is available.

3. Conclusions

In conclusion, we have presented a method for rapidly generating hierarchical TiO_2-doped SiO_2 microcapsules with low concentrations of TiO_2 nanoparticles distributed throughout the shells using simple mesofluidic T-junction devices. The hierarchical architecture was achieved without the use of additives such as inorganic salts [5]. Furthermore, we provided gentle, flow-based methods for quickly decorating the microparticles with additional TiO_2 nanocrystallites (~0.2 to 3.5 wt. %) or a variety of other transition metal oxide nanoparticles. Dye degradation experiments demonstrated that the titania nanoparticles were active and accessible for catalyzing photochemistry. We envision that these microcapsules have potential in various applications, from pigments and fillers to adsorption and photocatalysis, which we have demonstrated here. Further efforts are underway to investigate the formation of other composite, inorganic microcapsules using this simple device and to utilize the aforementioned coating methods to obtain hollow shells with tunable chemical and physical properties.

4. Experimental

4.1. Materials. Silicon tetrachloride ($SiCl_4$), tetraethyl orthosilicate (TEOS), titanium (IV) *n*-butoxide or tetrabutyl orthotitanate (TBOT), absolute ethanol, isopropanol, *t*-butanol, and glycerol were used as purchased without further purification. Commercially available laboratory tubing (PVC 1/16″ or 1/32″ i.d. and PFA 1/4″ i.d), minicolumns (Promega Corp.), and blunt-tipped needles were used as purchased.

4.2. Device Fabrication. The capsule-forming device was constructed from PVC laboratory tubing (1/32″ i.d.). The main channel was intersected with a 22-gauge flat-tipped needle. This needle was positioned such that the outlet (the tip) was directly in the center of the tubing creating a modified T-junction which we found to be critical to the droplet formation as the disperse phase rapidly polymerizes upon contact with the tubing walls leading to clogging of the device. Droplet formation was observed with the naked eye, and the interfacial reaction solidified the capsules within the 45-cm long section of tubing following the T-junction (device was used at room temperature).

4.3. Preparation of Continuous-Phase Solutions. The 80:20 glycerol–H_2O continuous phase was prepared by adding 40 mL of deionized water to 160 mL of glycerol and stirring until homogeneous (~1 h).

4.4. Preparation of Disperse-Phase Solutions. Precursor solutions were prepared by adding the liquid components successively to a dry glass vial under a nitrogen atmosphere. The order of addition was performed as follows: $SiCl_4$, tetraethylorthosilicate (TEOS), *t*-butanol, and titanium (IV) *n*-butoxide. For example, a formulation containing 1.8–2.5 mol % titanium (IV) *n*-butoxide was prepared by adding $SiCl_4$ (0.5 mL,), TEOS (0.93 mL), *t*-butanol (0.12 mL), and Ti (IV) *n*-butoxide (TBOT; 62–70 μL) to a dry glass 7-mL vial under inert atmosphere (molar ratio: 1.0:0.93:0.06:0.05). The solutions were stirred until homogeneous before use.

4.5. Synthesis of TiO_2-Doped SiO_2 Microcapsules. Continuous and disperse-phase solutions were loaded into plastic syringes, and both materials were pumped into the reaction by action of a syringe pump. The disperse phase (10–75 μL/min) was introduced perpendicularly to the continuous phase (0.3–3 mL/min), leading to the formation of monodisperse droplets. The size of the droplets could be controlled by altering the relative flow rates of the two phases. The microcapsules were collected in a large beaker containing continuous-phase solution. The microcapsules were isolated and washed with several aliquots of ethanol followed by deionized water and then isopropanol.

4.6. Surface Decoration of TiO_2-Doped SiO_2 Microcapsules. Washed capsules were loaded into a small cartridge constructed from a segment of PFA tubing (Figure 1) capped with Wizard® minicolumn filters (Promega Corp.). Capsule decoration was achieved by first activating surface hydroxyl groups by passing ethanol, made basic (pH~8–9) by addition of 1 M NaOH, through the packed bed (1 mL/min; total volume, ~10 mL). The capsules were then washed with fresh ethanol. Decoration with additional TiO_2 was achieved by passing a 0.15-M solution of TBOT in ethanol through the cartridge at 75 °C (0.200 mL/min; 4 h). Next, the capsules were rinsed with 20:1 ethanol–deionized water before being washed with isopropanol, collected, and dried at 120 °C. An alternative continuous-flow procedure was performed without pretreating the capsules with basic ethanol. Here, the flow rate of the 0.15 M TBOT solution was lowered to 0.100 mL/min (total reaction time of 5 h). Additionally, the capsules were annealed at temperatures up to 900 °C for 5 h to generate crystalline phases desirable for various applications. For low–evaporation surface coating, the cartridge of capsules was subjected to rinsing with 2 mL of 0.075–0.5 M TBOT in ethanol (repeated rinse, flowing the opposite direction of first rinse) followed by evaporation of solvent using air flow (~5 min; 2.5 min in each direction). This process was repeated 3–12× before rinsing with deionized water (5 mL) and isopropanol (5 mL), and then drying using air flow (~2 psi).

4.7. Characterization. The morphology of the microcapsules was examined by optical and scanning electron microscopy (SEM) using a Leica DL IM and LEO/ZEISS microscope model GEMINI 1530VP (30 kV) equipped with a low vacuum VPSE detector, respectively. Elemental analysis was performed using the EDX detector from Bruker with Software pack Esprit 1.9.4. Room temperature powder X-ray diffraction (PXRD) was

carried out on a PANalytical X'Pert Pro diffractometer with an X'Celerator detector using Cu Kα radiation (λ=1.54187 Å). Infrared spectroscopy of the microcapsules was performed using a Nicolet 380 FT-IR spectrometer and KBr pellets (30 mg per pellet; 2 wt. % sample). NMR spectroscopy was performed on an Agilent Technologies 400-MR DD2 400 MHz spectrometer using a 5-mm OneNMR probe.

4.8. Photochemical Degradation of Methyl Orange (MO). Full experimental details are in the supporting information. Briefly, reactions were run in a quartz, demountable flow cell (Starna Cells, Inc, 8 × 38 mm, 0.50 mm path length). Flow was achieved using a peristaltic pump attached to the cell with PVC laboratory tubing (1/8″ i.d., 90 cm total). UV radiation was supplied by a 1.0-kW Xe lamp (Oriel Labs) focused into the flow cell by a dichroic mirror and lens assembly (Oriel Labs) with a total beam length of 45.7 cm. For all experiments, the initial concentration of MO was 2.75×10^{-4} M. Titania-coated microcapsules (8.5 mg total, 300 μg TiO_2) were immobilized to the flow cell via sticky tape, or commercial TiO_2 (300 μg, Degussa P-25, 85% anatase, 15% rutile) was suspended in the aqueous solution (10.0 mL). The concentration of MO was measured versus time of irradiation via UV–vis spectroscopy (ε_{480} = 22,177/M/cm).

4.9. Synthesis of Other Transition Metal Oxide Composites. Full experimental details are in the supporting information. Briefly, saturated methanolic solutions of each salt were passed through a cartridge loaded with pure silica (undecorated) microcapsules. Then, the solvent was evaporated under a flow of air at room temperature and for 1 h at 350 °C. The deposition of soluble precursors was repeated, and then the samples were calcined at 660 °C for 5 h to yield the metal oxide–silica composites.

Acknowledgement. This material is based upon work supported by the National Science Foundation under grant numbers CHE-1152020, CHE-1229021, and DMR-1410387. We would also like to acknowledge the DoD (DOTC 13-01-INIT518) and Chemring, Inc. for financial support. G.O.G. acknowledges Romeo Saliwan-Neumann for SEM measurements. G.O.G. also acknowledges the Federal Institute for Materials Research and Testing (BAM) for instrumental support and Max Planck Society for financial support. We thank Prof. Steven Szczepankiewicz for helpful discussions.

Supporting Information

Electronic Supplementary Material (ESM) (additional experimental details, additional powder X-ray diffraction data, detailed flow cell procedures and data, and additional SEM and TEM images) associated with this article can be found in the online version at doi:10.1556/1846.2016.000002.

Abbreviations

TEOS: tetraethoxysilane
TBOT: tetrabutylorthotitanate
SEM: scanning electron microscopy
TEM: transmission electron microscopy
EDX: energy-dispersive X-ray
PXRD: powder X-ray diffraction
FT-IR: Fourier transform infrared

References

1. Lou, X. W.; Archer, L. A.; Yang, Z. *Adv. Mater.* **2008**, *20*, 3987–4019.
2. Liu, J.; Liu, F.; Gao, K.; Wu, J.; Xue, D. *J. Mater. Chem.* **2009**, *19*, 6073–6084.
3. Hu, J.; Chen, M., Fang, X.; Wu, L. *Chem. Soc. Rev.* **2011**, *40*, 5472–5491.
4. Chen, M.; Ye, C.; Zhou, S.; Wu, L. *Adv. Mater.* **2013**, *25*, 5343–5351.
5. Fujiwara, M.; Shiokawa, I.; Sakakura, I.; Nakahara, Y. *Langmuir* **2010**, *26*, 6561–6567.
6. Song, X.; Gao, L. *Langmuir* **2007**, *23*, 11850–11856.
7. Lan, W.; Li, S.; Xu, J.; Luo, G. *Langmuir* **2011**, *27*, 13242–13247.
8. Yao, L.-F.; Shi, Y.; Jin, S.-R.; Li, M.-J.; Zhang, L.-M. *Mater. Res. Bull.* **2010**, *45*, 1351–1356.
9. Zhao, W.; Feng, L.; Yang, R.; Zheng, J.; Li, X. *Appl. Catal. B.* **2011**, *103*, 181–189.
10. Li, X.; John, V. T.; He, G.; He, J.; Spinu, L. *J. Mater. Chem.* **2012**, *22*, 17476–17484.
11. Hanprasopwattana, A.; Srinivasan, S.; Sault, A. G.; Datye, A. K. *Langmuir* **1996**, *12*, 3173–3179.
12. Guo, N.; Liang, Y.; Lan, S.; Liu, L.; Ji, G.; Gan, S.; Zou, H.; Xu, X. *Appl. Surf. Sci.* **2014**, *305*, 562–574.
13. Son, S.; Hwang, S. H.; Kim, C.; Yun, J. Y.; Jang, J. *ACS Appl. Mater. Interfaces* **2013**, *5*, 4815–4820.
14. Dahl, M.; Liu, Y.; Yin, Y. *Chem. Rev.* **2014**, *114*, 9853–9889.
15. Caruso, F.; Shi, X.-Y.; Caruso, R. A.; Susha, A. *Adv. Mater.* **2001**, *13*, 740–744.
16. Caruso, R. A.; Susha, A.; Caruso, F. *Chem. Mater.* **2001**, *13*, 400–409.
17. Wu, W.; Cao, S.; Yuan, X.; Zhao, Z.; Fang, L. *J. Porous Mater.* **2012**, *19*, 913–919.
18. Li, W.; Coppens, M.-O. *Chem. Mater.* **2005**, *17*, 2241–2246.
19. Li, D.; Guan, Z.; Zhang, W.; Zhou, X.; Zhang, W. Y.; Zhuang, Z.; Wang, X.; Yang, C. J. *ACS Appl. Mater. Interfaces* **2010**, *2*, 2711–2714.
20. Wan, J. Stone, H. A. *Langmuir* **2012**, *28*, 37–41.
21. Zhao, C.-X.; Middelberg, A. P. J. *Microfluid. Nanofluid.* **2013**, *14*, 703–709.
22. Fujiwara, M.; Shiokawa, K.; Tanaka,Y.; Nakahara, Y. *Chem. Mater.* **2004**, *16*, 5420–5426.
23. Steinbacher, J. L.; McQuade, D. T. *J. Polym. Sci. A* **2006**, *44*, 6505–6533.
24. McQuade, D. T.; Seeberger, P. H. *J. Org. Chem.* **2013**, *78*, 6384–6389.
25. Steinbacher, J. L.; Moy, R. W. Y.; Price, K. E.; Cummings, M. A.; Roychowdhury, C.; Buffy, J. J.; Olbricht, W. L.; Haaf, M.; McQuade, D. T. *J. Am. Chem. Soc.* **2006**, *128*, 9442–9447.
26. Miller, L. Z.; Steinbacher, J. L.; Houjeiry, T. I.; Longstreet, A. R.; Woodberry, K. L.; Gupton, B. F.; Chen, B.; Clark, R.; McQuade, D. T. *J. Flow Chem.* **2012**, *2*, 92–102.
27. Serra, C. A.; Khan, I. U.; Chang, Z.; Bouquey, M.; Muller, R.; Kraus, I.; Schmutz, M.; Vandamme, T.; Anton, N.; Ohm, C.; Zentel, R.; Knauer, A.; Köhler, M. *J. Flow Chem.* **2013**, *3*, 66–75.
28. Chang, Z.; Serra, C. A.; Bouquey, M.; Prat, L.; Hadziioannou, G. *Lab Chip* **2009**, *9*, 3007–3011.
29. Brinker, C. J.; Scherrer, G. W. *Sol–Gel Science: The Physics and Chemistry of Sol–Gel Processing*; Academic Press, Inc.: Boston, 1990; pp. 42–59.
30. Stöber, W.; Fink, A.; Bohn, E. *J. Coll. Interf. Sci.* **1968,** *26*, 62–69.
31. Lee, D. W.; Ihm, S. K.; Lee, K. H. *Chem. Mater.* **2005**, *17*, 4461–4467.
32. Mariscal, R.; Lopez-Granados, M.; Fierro, J. L. G.; Sotelo, J. L.; Martos, C.; Van Grieken, R. *Langmuir* **2000**, *16*, 9460–9467.
33. Gibbs, B. F.; Kermasha, S.; Alli, I.; Mulligan, C. N. *Int. J. Food Sci. Nutr.* **1999**, *50*, 213–224.
34. Li, J.; Jing, Z.; Zha, F.; Yang, Y.; Wang, Q.; Lei, Z. *ACS Appl. Mater. Interfaces* **2014**, *6*, 8868–8877.
35. Faustini, M.; Boissière, C.; Nicole, L.; Grosso, D. *Chem. Mater.* **2014**, *26*, 709–723.
36. Li, C.; Koenigsmann, C.; Ding, W.; Rudshteyn, B.; Ke R. Yang, K. R.; Regan, K. P.; Konezny, S. J.; Batista, V. S.; Brudvig, G. W.; Schmuttenmaer, C. A.; Kim, J.-H. *J. Am. Chem. Soc.* **2015**, *137*, 1520–1529.
37. Hashimoto, K.; Irie, H.; Fujishima, A. *Jpn. J. Appl. Phys.* **2005**, *44*, 8269–8285.
38. Hurum, D. C.; Agrios, A. G.; Gray, K. A.; Rajh, T.; Thurnauer M. C. *J. Phys. Chem. B* **2003**, *107*, 4545–4549.
39. Szczepankiewicz, S. H.; Colussi, A. J.; Hoffmann, M. R. *J. Phys. Chem. B* **2000**, *104*, 9842–9850.
40. Meshram, S. P.; Adhyapak, P. V.; Mulik, U. P.; Amalnerkar, D. P. *Chem. Eng. J.* **2012**, *204–206*, 158–168.
41. Guo, M. Y.; Liu, F.; Tsui, J.; Voskanyan, A. A.; Ng, A. M. C.; Djurisic, A. B.; Chan, W. K.; Chan, K.-Y.; Liao, C.; Shih, K.; Sura, C. *J. Mater. Chem. A* **2015**, *3*, 3627–3632.
42. Liu, H.; Zhang, S.; Liu, Y.; Yang, Z.; Feng, X.; Lu, X.; Huo, F. *Small* **2015**, *11*, 3130–3134.
43. Li, W.-Y.; Xu, L.-N.; Chen, J. *Adv. Funct. Mater.* **2005**, *15*, 851–857.
44. Sun, X.; You, R.; Hu, X.; Mo, J.; Xiong, R.; Ji, H.; Li, X.; Cai, S.; Zheng, C.; Meng, M. *RSC Adv.* **2015**, *5*, 35524–35534.
45. Wang, X.; Zhang, L.; Ni, Y.; Hong, J.; Cao, X. *J. Phys. Chem. C* **2009**, *113*, 7003–7008.
46. Mondal, A. K.; Chen, S.; Su, D.; Kretschmer, K.; Liu, H.; Wang, G. *J. Alloys Compd.* **2015**, *648*, 732–739.
47. Hosseinpour, M.; Fatemi, S.; Ahmadi, S. J. *Fuel* **2015**, *159*, 538–549.
48. Kim, J.; Piao, Y.; Lee, N.; Park, Y. I.; Lee, I.-H. Lee, J.-H.; Paik, S. R.; Hyeon, T. *Mater.* **2010**, *22*, 57–60.
49. Ling, D.; Gao, L.; Wang, J.; Shokouhimehr, M.; Liu, J.; Yu, Y.; Hackett, M. J.; So, P. K.; Zheng, B.; Yao, Z.; Xia, J.; Hyeon, T. *Chem. Eur. J.* **2014**, *20*, 7916–7921.
50. Fatima, B.; Jabeen, F.; Padashbarmchic, Z.; Najamul-Haq, M. *RSC Adv.* **2015**, 5, 23658–23665.